Received: 31 October 2018 | Revised: 10 January 2019 | Accepted: 24 January 2019

DOI: 10.1111/jace.16364

ORIGINAL ARTICLE

Journal of the American Ceramic Society

Defect-fluorite $Gd_2Zr_2O_7$ ceramics under helium irradiation: Amorphization, cell volume expansion, and multi-stage bubble formation

Zhangyi Huang[1,2] | **Nannan Ma**[1] | **Jianqi Qi**[1,2,3] | **Xiaofeng Guo**[4,5] | **Mao Yang**[1,2] | **Zhe Tang**[1] | **Yutong Zhang**[1] | **Yong Han**[6] | **Di Wu**[4,5,7,8] | **Tiecheng Lu**[1,2,3]

[1]College of Physical Science and Technology, Sichuan University, Chengdu, China
[2]Key Laboratory of Radiation Physics and Technology of Ministry of Education, Sichuan University, Chengdu, China
[3]Key Laboratory of High Energy Density Physics of Ministry of Education, Sichuan University, Chengdu, China
[4]Alexandra Navrotsky Institute for Experimental Thermodynamics, Washington State University, Pullman, Washington
[5]Department of Chemistry, Washington State University, Pullman, Washington
[6]Department of Physics and Astronomy, Iowa State University, Ames, Iowa
[7]The Gene and Linda Voiland School of Chemical Engineering and Bioengineering, Washington State University, Pullman, Washington
[8]Materials Science and Engineering, Washington State University, Pullman, Washington

Correspondence
Jianqi Qi, College of Physical Science and Technology, Sichuan University, Chengdu, China.
Email: qijianqi@scu.edu.cn
and
Di Wu, Alexandra Navrotsky Institute for Experimental Thermodynamics, Washington State University, Pullman, WA.
Email: d.wu@wsu.edu
and
Tiecheng Lu, College of Physical Science and Technology, Sichuan University, Chengdu, China.
Email: lutiecheng@scu.edu.cn

Funding information
Science and Technology Innovation Team of Sichuan Province, Grant/Award Number: 15CXTD0025; Key Applied Basic Research of Sichuan Province, Grant/Award Number: 2017JY0329; Washington State University; National Natural Science Foundation of China, Grant/Award Number: 11505122 and 11775152; Alexandra Navrotsky Institute for Experimental Thermodynamics

Abstract

Here, we report a study on the radiation resistance enhancement of $Gd_2Zr_2O_7$ nanograin ceramics, in which amorphization, cell volume expansion, and multi-stage helium (He) bubble formation are investigated and discussed. $Gd_2Zr_2O_7$ ceramics with a series of grain sizes (55-221 nm) were synthesized and irradiated by 190 keV He ion beam up to a fluence of 5×10^{17} ions/cm^2. Both the degree of post irradiation cell volume expansion and the amorphization fraction appear to be size-dependent. As the average grain size evolves from 55 to 221 nm, the degree of post irradiation cell volume expansion increases from 0.56% to 1.02%, and the amorphization fraction increases from 6.8% to 11.1%. Additionally, the threshold He concentrations (at.%) of bubbles at different formation stages and locations, including (a) bubbles at grain boundary, (b) bubble-chains, and (c) ribbon-like bubbles within the grain, are all found to be much higher in the nanograin ceramic (55 nm) compared with that of the submicron sample (221 nm). We conclude that grain boundary plays a critical role in minimizing the structural defects, and inhibiting the multi-stage He bubble formation process.

KEYWORDS
degradation, interfaces, radioactive waste

1 | INTRODUCTION

Crystalline $A_2B_2O_7$ oxides with defect fluorite or pyrochlore phases have great potential to be applied as synthetic rocks for high-level nuclear waste immobilization (SYNROC). Radioactive actinides may be confined and immobilized include Pu, Am, and Cm.[1–3] However, typically, under highly radioactive environments, the irradiation-induced amorphization damage the ceramic waste form structures resulting in poor chemical durability and/or radioactive nuclide release.

The irradiation resistance properties of $A_2B_2O_7$ materials to amorphization have been systematically studied.[4–6] $Gd_2Zr_2O_7$ is often considered as a radiation tolerant $A_2B_2O_7$ oxide, which cannot be completely amorphized even at dose up to 100 dpa.[3–5] At a fluence of 1×10^{16} Xe^{20+}/cm, more than 25% $Gd_2Zr_2O_7$ is amorphized.[2,7] In addition, other than the deleterious effect induced by structural damage, He atoms undergo a continuous accumulation due to α-decay, forming He bubbles in the $Gd_2Zr_2O_7$ host matrix, and causing swelling and surface blistering.[8,9] Moreover, He accumulation may also generate mechanical stress, which results in cracking, thereby increasing the interfacial contact of radionuclides with ground water, and reducing the chemical durability of the waste forms.[8]

Recently, nanostructured materials with high grain boundary (GB) density were found to be promising waste form candidates to minimize the detrimental radiation defects induced by accumulation of structural damage and impurity (He atoms). For instance, enhanced radiation resistance to amorphization was observed for nanostructured $MgGa_2O_4$, yttria stabilized zirconia (YSZ), and $Gd_2(Ti_{0.65}Zr_{0.35})_2O_7$ powder.[10–14] Additionally, improved radiation tolerance to swelling and hardening caused by He bubble was also observed for nanostructured steel, tungsten film, and Fe–Cr–Ni alloy.[15–17] Nevertheless, thus far, the exact role of GB and/or grain size in (a) structural orderness or amorphization, (b) cell volume expansion, and (c) bubble formation induced by He irradiation for the $A_2B_2O_7$ ceramic, remains unclear.

Here, we present a study on He ion radiation resistance behavior of $Gd_2Zr_2O_7$ ceramics to amorphization, unit cell swelling, and multi-stage He bubble formation as the sample grain size increases from nanoscale (55 nm) to submicron scale (221 nm). The starting material we used, nanocrystalline $Gd_2Zr_2O_7$ powder, has a pure defect fluorite phase. It was synthesized by a solvothermal assisted co-precipitation method followed by calcination at 800°C in air for 4 hours.[18] Subsequently, the as obtained $Gd_2Zr_2O_7$ powders were consolidated into ceramic pellets by field assisted sintering technique (FAST) using a LABOX-325 system (Sinter Land Inc., Ameike, Nagaoka, Niigata, Japan). We determined the average grain sizes of samples sintered at 1170°C (55 nm), 1240°C (70 nm), 1320°C (123 nm), and 1400°C (221 nm) for 5 minutes using a statistical measurement from fractured cross-section images employing Nano Measure software (Nano Measurer 1.2, Fudan University, Shanghai, China). These $Gd_2Zr_2O_7$ samples with a series of grain sizes were double-side polished using fine metallographic abrasive paper and diamond paste until reaching surface roughness less than 10 nm.

2 | EXPERIMENTAL METHODS

The bulk densities of all $Gd_2Zr_2O_7$ samples were determined by the Archimedes method using water as the media. These $Gd_2Zr_2O_7$ ceramics were irradiated with 190 keV He ion beam to the fluence of 5×10^{17} ions/cm^2 at room temperature using a 200 keV ion implanter (LC22-100-01; Beijing Zhongkexin Electronics Equipment Co., Ltd, Beijing, China) at Center for Ion Beam Application, Wuhan University, Wuhan, Hubei province, China. Peak damage (displacement per atom) and He concentration (atomic percentage) were examined by SRIM 2008 (Stopping and Range of Ions in Matter, SRIM Co., Chester, MD, 2008) using threshold displacement energies of 72 (Gd), 121 (Zr), and 41 (O) eV. [19]-incidence X-ray diffraction (GIXRD) measurement (Bruker AXS D8 Advances X-ray diffractometer, Bruker AXS GmbH, Karlsruhe, Germany) with Cu Ka radiation, $\lambda = 1.5406$ Å was conducted at an incident angle of 6° according to Taylor's experiments, which were very nearly identical with our irradiation conditions, to investigate the phase evolution of the samples upon irradiation.[8] In Taylor's experiments, $Gd_2Zr_2O_7$ ceramics with relative densities of 95%-97% were irradiated by 200 keV He ion. The incident angle chosen was 6^o. The non-irradiated side of each ceramic pellet was also examined with GIXRD under the same experimental condition. Whole-pattern profile fitting of the diffraction data was performed to obtain the lattice parameters, diffraction peak areas, and FWHM (full width at half maximum) of each sample before and after irradiation. Focused ion beam (FIB) was employed to prepare the cross-sections of the irradiated samples. Transmission electron microscopy (TEM, FEI Tecnai G^2 F20 TWIN, FEI Company, Hillsboro, OR, USA) was performed to elucidate the post He irradiation sample microstructural evolutions. The grain size and the width of GB were derived from a statistical measurement given by the Nano Measure software. For each statistical data, more than 20 grains and 5 GBs were measured.

3 | RESULTS AND DISCUSSIONS

The relative densities of all samples were measured using the Archimedes method with water as the media. Specifically, the relative densities are 91.3% (55 nm), 94.8% (70 nm), 97.5%

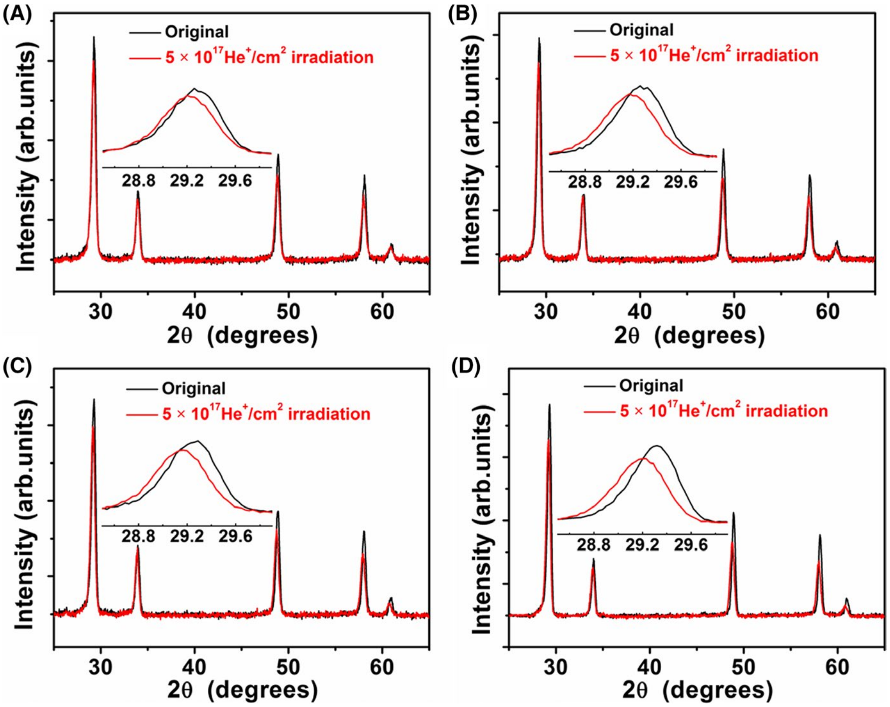

FIGURE 1 GIXRD patterns of $Gd_2Zr_2O_7$ ceramics prior and post He irradiation: A, 55 nm; B, 70 nm; C, 123 nm; and D, 221 nm [Colour figure can be viewed at wileyonlinelibrary.com]

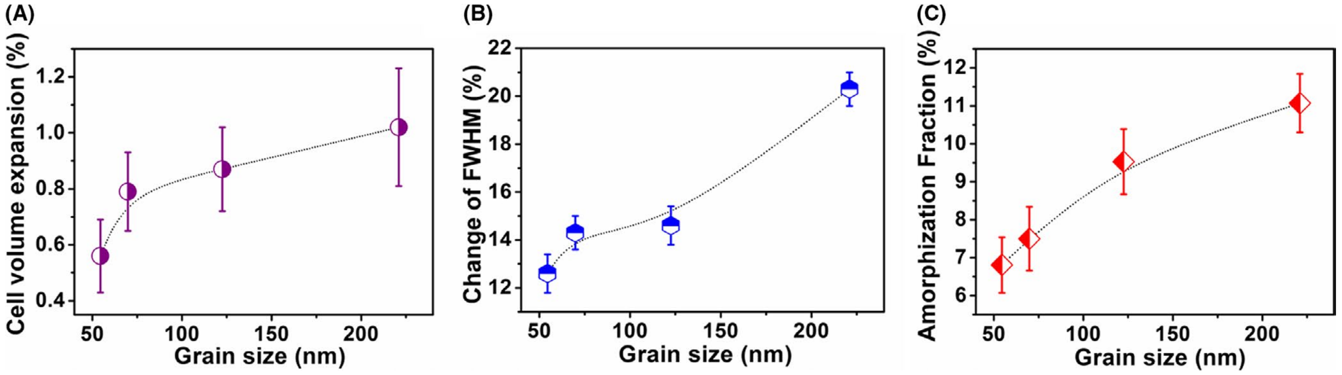

FIGURE 2 Post irradiation (A) cell volume expansion, (B) FWHM increase, and (C) degree of amorphization for $Gd_2Zr_2O_7$ ceramics as grain size varies. FWHM, full width at half maximum [Colour figure can be viewed at wileyonlinelibrary.com]

(123 nm), and 98.4% (221 nm). Figure 1 shows the GIXRD patterns of $Gd_2Zr_2O_7$ ceramics (55-221 nm) before and after He irradiation at 5×10^{17} ions/cm^2. All the samples share a pure defect-fluorite phase before irradiation, and such structure is well-retained after irradiation. Interestingly, left shift was observed for all irradiated ceramic pellets, indicating lattice expansion induced by He implantation. In addition, intensity reduction and peak broadening were observed for all post irradiation samples.

Interestingly, left shifts, intensity reduction, and peak broadening appear to be grain size-dependent (Figure 2). Left shifts of diffraction peaks suggest lattice expansion. It is known that vacancy and vacancy clusters induce stress field, which leads to lattice expansion.[20, 21] We calculated the lattice parameter increase and cell volume expansion. Surprisingly, as the average grain size increases from 55 to 221 nm, the degree of post irradiation cell volume expansion increases from 0.56% to 1.02% (see Figure 2A). Additionally, the FWHM increases 12.6% for nanograin (55 nm) ceramic, and 20.3% for the sub-micron ceramic (221 nm, see Figure 2B). It is very likely that the diffuse scattering induced by formation of damaged structure during irradiation process account for the peak broadening and intensity reduction.[11,22] Since the diffraction peak of the irradiation induced amorphous phase is usually significantly broader, the irradiated areas observed in our study are very likely to be partially amorphized. Thus, we derived the amorphous phase fraction (f_A) from the net area of diffraction peak using the following equation[7]:

$$f_A = 1 - \frac{\sum_{i=1}^{n} \frac{A_i^{\text{irradiated}}}{A_i^{\text{unirradiated}}}}{n}$$

$A_i^{\text{irradiated}}$ and $A_i^{\text{unirradiated}}$ represent the areas of the ith GIXRD peaks of the irradiated and non-irradiated sides, respectively. n is the number of diffraction peaks. The post-irradiation amorphous phase fraction is plotted as a function of average grain size in Figure 2C. Specifically, for the 55 and 221 nm samples, 6.8% and 11.1% of the crystalline phase were amorphized after irradiation, respectively.

TEM was employed to elucidate the size-dependent microstructural evolution of $Gd_2Zr_2O_7$ ceramics upon He irradiation (see Figures 3 and 4). For the sub-micron ceramic sample, a clearly damaged region can be observed (see Figure 3A). Interestingly, in the TEM image of the nanograin ceramic sample, such damage region is not as clearly resolved as that of the sub-micron sample (see Figure 3B). The TEM images in Figure 3B,D present the areas with the most severe damage. Images at higher magnification are also shown in Figure 3A,C. For the sub-micron ceramic, the region with more damage may indicate higher degree of post He radiation structural degradation in the inner grains. The SAED patterns and FFT images presented in Figure 4A-C and D-F suggest that both the sub-micron and nanograin $Gd_2Zr_2O_7$ retain their crystalline structures (partial order structure) at a dose up to 6.3 dpa. However, in the HRTEM images of non-irradiated substrate (Figure 4), the upper irradiated layer (about 1.8 dpa) and the peak damaged layer (about 6.3 dpa) of both the sub-micron (Figure 4A-C) and the nanograin (Figure 4D-F) ceramics, the radiation defects mainly present in the form of vacancy. The concentration of vacancy-type defects or defect clusters increases as the dpa value increases. Meanwhile, the average size of defect cluster (see the yellow circles in Figure 4) clearly increases in the submicron sample yet appears to be the same in nanograin ceramic. Moreover, the increasing local concentration (number) and size of vacancy clusters can be distinguished as grain size increases. According to an earlier study, the vacancy-type defects dominate the major radiation defect forms inside grains is because of the much weaker mobility compared with that of interstitials, which are eventually absorbed by the GBs or are migrated into the material surface.[23–25] Furthermore, the total defect concentration increases as the grain size increases, in which the GBs act as neutralizer for both vacancies and interstitials.[24]

The detail behaviors of implanted He in submicron and nanograin ceramics were presented in Figure 5. In a thermodynamic sense, GB is a preferred location to trap implanted He atoms.[10] Specifically, GB segregation is first observed at ~300 nm away from the surface, which increases the width of GB to ~1.8 nm (corresponding to 1.7 at.% He in the SRIM calculated concentration profile, see Figure 5A and inset). Such distinct difference originates from coalescence behavior of He bubbles which leads to the formation of interconnected channels parallel with the GB[26] (see the red arrows in Figure 5). Within the near-surface region (~300 nm), the inner grains

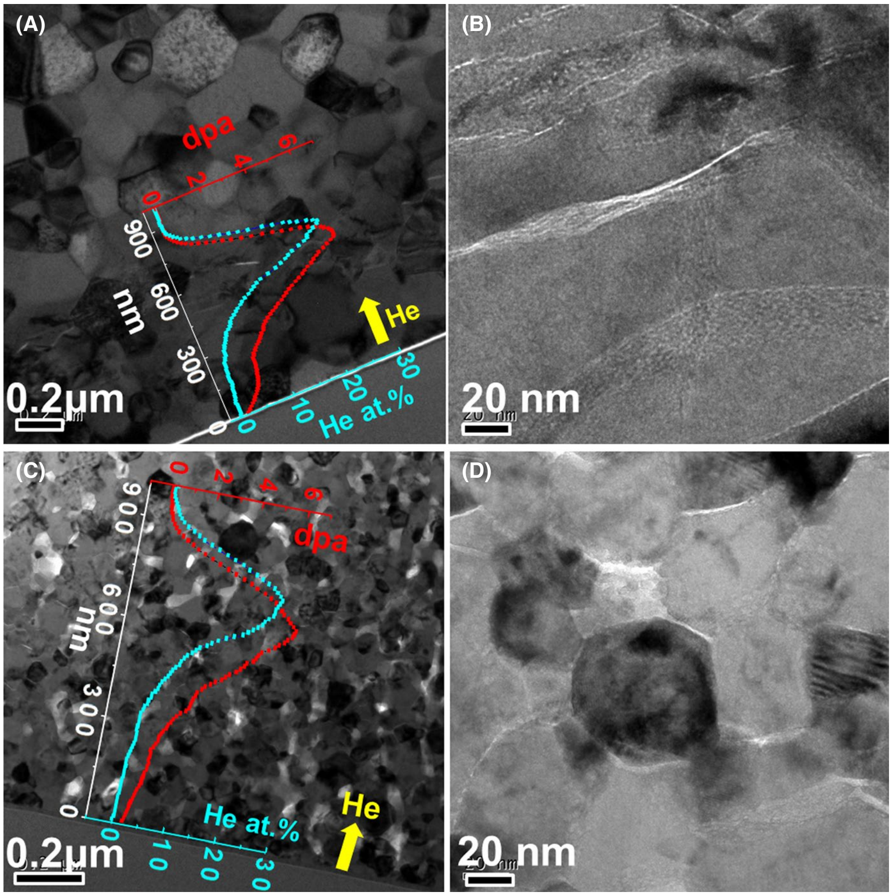

FIGURE 3 Cross-sectional TEM images of the post-He irradiation (A) sub-micron, (C) nanograin $Gd_2Zr_2O_7$ ceramics. (B) and (D) are the TEM images of mostly damaged areas in (A) and (C) at higher magnification, respectively. The inset of A and C shows the depth profiles of radiation damage in dpa and the He concentration (at.%) obtained from SRIM simulation [Colour figure can be viewed at wileyonlinelibrary.com]

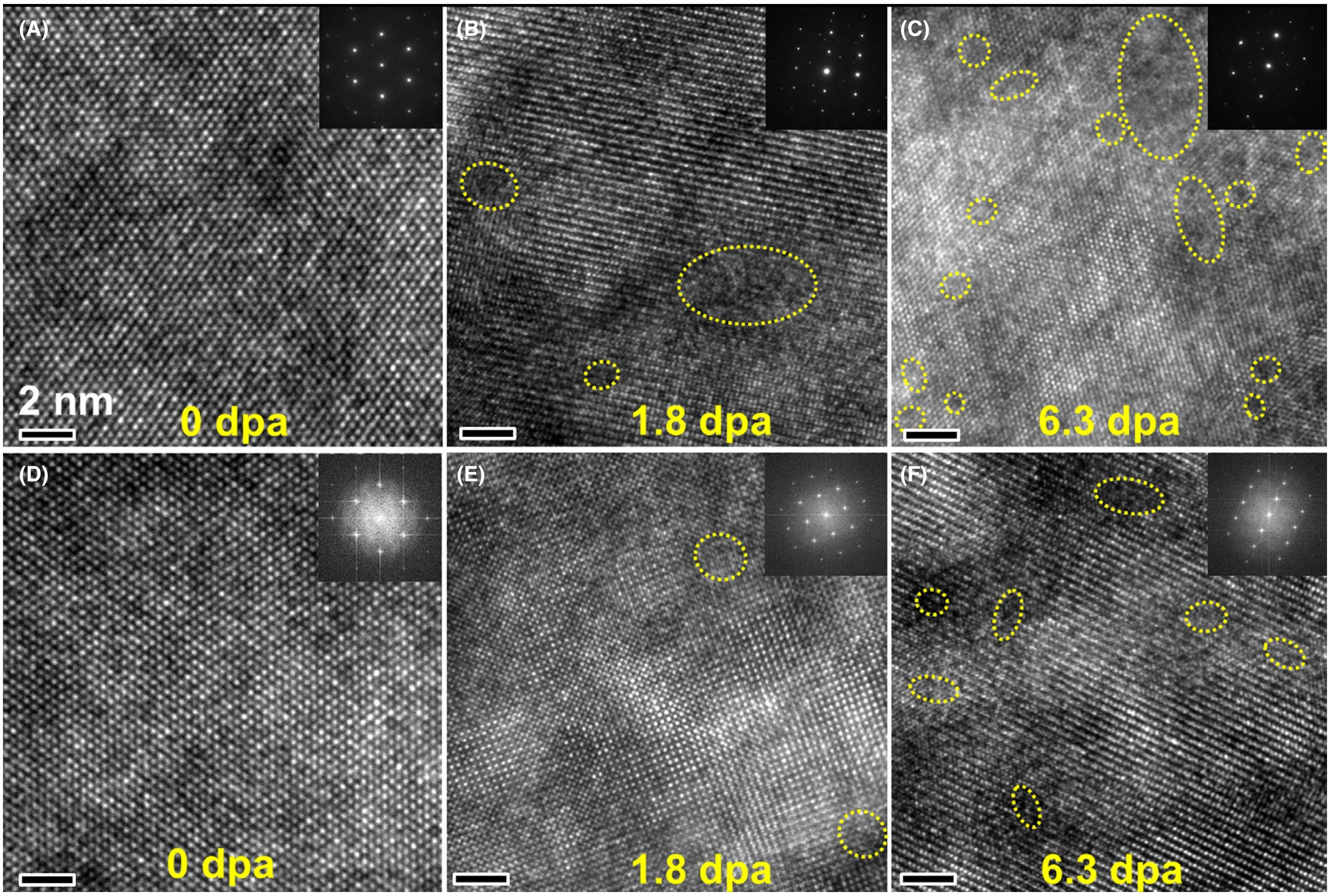

FIGURE 4 HRTEM images and corresponding SAED patterns of $Gd_2Zr_2O_7$ ceramic with different average grain size (A–C) 55 nm and (D–F) 221 nm, recorded from the non-irradiated sample (~0 dpa), the upper irradiated layer (~1.8 dpa), and the peak damaged layer (~6.3 dpa) [Colour figure can be viewed at wileyonlinelibrary.com]

and GBs which are perpendicular to the external surface are bubble-free. Only the inner grain appears to have no He bubble at approximately 300 nm away from external particle surface. Around the peak damaged area (see Figure 5B,C), the formation of He bubble chains (see dark blue arrows) and ribbon-like He bubbles inside grains (see cyan arrows) was observed at depths of ~435 and ~590 nm (corresponds to 5.9 and 19.2 at.% He), respectively. Besides, the maximum width of the GB with continuously distributed He bubbles increases to 3.9 nm, and the width of the He bubble chains inside grains is about 1.4 nm (measured by Nano Measure software). The unirradiated substrate appears to have no bubbles or bubble chains (see Figure 5D).

Figure 6 presents the width of GB with He bubbles as a function of He concentration (at.%). As the He concentration increases, the width of GB with He bubble increases accordingly. In addition, for the same He concentration as the average grain size increases, the width of GB with He bubble increases. Furthermore, the behavior of He bubbles in nanograin and submicron ceramics have four major distinct differences (highlighted in Figure 5E-H): (a) Nanograin sample has much higher He concentration leading to formation of He bubble along GB, He bubble chain inside grain, and ribbon-like He bubble inside grain, respectively. We also present corresponding TEM images and calculated SRIM profile, and corresponding results obtained from TEM images and SRIM calculated profile are listed in Table 1. (b) Nanograin ceramic features much more He bubble along the GB around peak damaged area; (c) Nanograin sample posseses much thinner maximum GB width distributed with He bubbles (~2.4 nm). (d) There is no ribbon-like He bubble within nanograin ceramic.

Shen[27] proposed a thermodynamic model, in which the differences in radiation damage behavior for nanograin and coarse-grained materials were interpreted and discussed. It is concluded that radiation damage is governed by the simultaneous and integrated effects of healing kinetics and thermodynamic stability.[27] On the one hand, the free energy of system increases as the grain size decreases. Such free energy depression decrease the energetic difference between the crystalline and corresponding amorphous phases, and significantly increases the probability of radiation induced phase transitions (amorphization). One example is that nanocrystalline ZrO_2 (<10 nm) is found to have stronger driving force

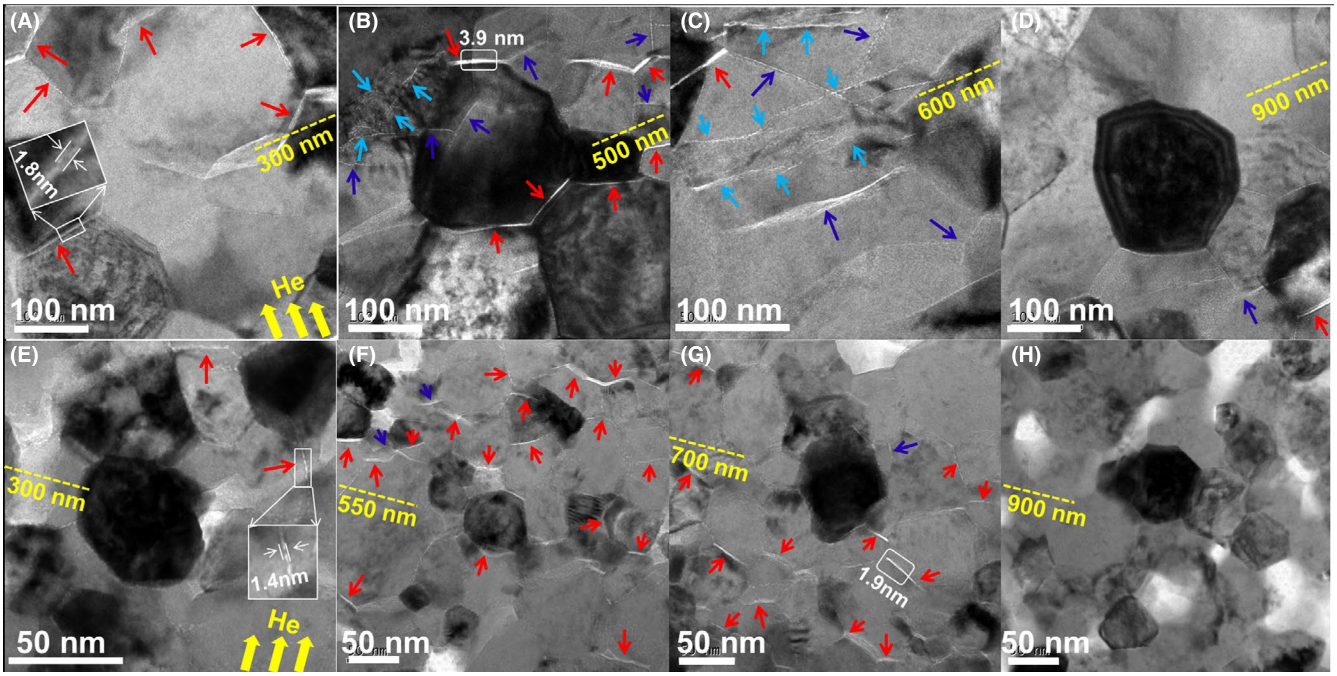

FIGURE 5 TEM images recorded at different depths (away from the surface) for post-He irradiation $Gd_2Zr_2O_7$ ceramics: A–D, 221 nm; E–H, 55 nm. The yellow dash lines are parallel to the external sample surface. The red, dark blue and cyan arrows point to (a) He bubble along GB, (b) He bubble chain inside grain and (c) ribbon-like He bubble inside grain, respectively [Colour figure can be viewed at wileyonlinelibrary.com]

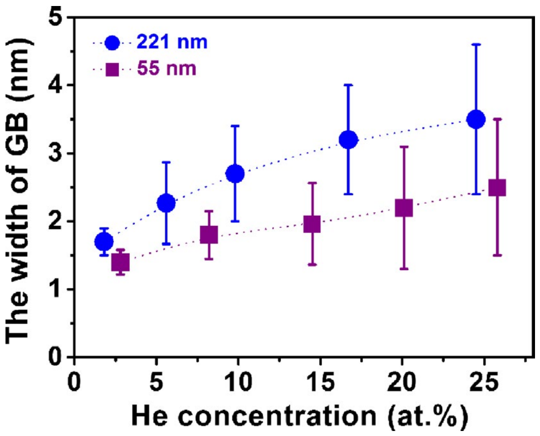

FIGURE 6 Width of grain boundary (GB) with He bubbles as a function of He concentration (at.%) [Colour figure can be viewed at wileyonlinelibrary.com]

TABLE 1 Threshold He concentrations (at.%) in submicron and nanograin $Gd_2Zr_2O_7$ ceramics to form multi-stage He bubble

Average grain size	221 nm	55 nm
He bubble along GB	1.7%	2.8%
He bubble chain inside grain	5.9%	15.2%
Ribbon-like He bubble	19.2%	>25.8%

toward amorphization.[28] On the other hand, GB can act as sink for point defects, promoting efficient localized annihilation of radiation damage via interstitial emission.[23] Once the interfacial area of GB is not significantly enough to impact the material stability, self-healing effect may counter-balance the instability induced by the GB energy. As reported earlier, nanocrystalline $MgGa_2O_4$ retains its crystallinity upon irradiation at 96 dpa. In contrast, bulk $MgGa_2O_4$ surfers from amorphization even at 24 dpa.[10] Considering such integrative effects, it is very likely that there is a grain size on nanoscale which leads to the best radiation resistance performance for $Gd_2Zr_2O_7$ nanoceramics. According to the GIXRD and TEM results, the 55 nm $Gd_2Zr_2O_7$ sample appears to have better radiation resistance to amorphization.

Other than grain size dependence, nanocrystalline materials also exhibit radiation-induced grain growth phenomena, which typically trigger material life-time decreases in radioactive environments.[29] For instance, the grain size of YSZ ceramic increases from 38 to 45 nm after treatment under irradiation, suggested by well-resolved GIXRD peak sharpening and direct TEM evidences.[11] Moreover, inter-granular cracks were observed in severely damaged region when nanograin samples (25 or 38 nm) were irradiated.[11] However, such phenomena were not observed in our study even under high fluence (5×10^{17} ions/cm^2), supported by the GIXRD peak broadening and directly identified micron-morphology in TEM images.

Comparing with inner grains, GBs are favored nucleation sites for He bubbles. Such irradiation induced bubbles prefer alignment and distribution along the GBs.[17] As the local concentration of He increases, the He bubble formation mechanism appears to have three distinct stages, including (a) He bubble formation along GB, (b) He bubble chain formation inside grain and (c) ribbon-like He bubble formation inside grain. This phenomenon is in excellent agreement with what was seen for YSZ ceramic.[26] Furthermore, the threshold He concentrations (at.%) for each bubble formation stage is found to be much higher for nanograin $Gd_2Zr_2O_7$ ceramics compared with the submicron samples. In other words, the nanograin ceramics have stronger capability to inhibit the formation and evolution of He bubbles. We conclude that one reason for hysteretic He bubble formation in nanograin ceramics is that the higher GB area enables effective He bubble distribution. On the other hand, the inner grain bubbles are generated by trapping He in structural voids.[30] Owing to the enhanced vacancy defect neutralization by larger GB areas, the void density is effectively reduced, leading to less small size He bubbles.

In our ongoing and future work, we plan to carefully examine the energetic stability (formation enthalpies) of fresh and post-irradiation $Gd_2Zr_2O_7$ ceramics studied in this work using various calorimetric techniques.

4 | CONCLUSIONS

In summary, the He irradiation behavior of $Gd_2Zr_2O_7$ ceramics with grain size from 55 to 221 nm was studied. Our results suggest that the irradiation induced amorphization and cell volume expansion behaviors of $Gd_2Zr_2O_7$ ceramics are grain size-dependent. Specifically, the nanograin ceramic (55 nm) presents the least degree of amorphization and cell volume expansion upon irradiation. Additionally, nanograin ceramics exhibit enhanced capability to inhibit multi-stage He bubble formation. As the average grain size evolves from 55 to 221 nm, the threshold He concentrations (at.%) for (a) bubble formation along GB, (b) bubble chain inside grain and (c) ribbon-like bubble inside grain increase from 1.7% to 5.9% and 19.2% to 2.8%, 15.2% to more than 25.8%, respectively. Compared with the submicron samples, much more He bubbles were observed to be enriched along the GBs, and much thinner maximum width of the GB were found to have He bubbles distributed for the in the nanograin ceramic. Moreover, irradiation induced grain growth and intergranular cracks were not observed for $Gd_2Zr_2O_7$ nanograin ceramics. We identified that 55 nm is the optimized size for $Gd_2Zr_2O_7$ nanograin ceramics with enhanced radiation tolerance and thermodynamic stability. Our study provides needed fundamental experimental data and general guidance to design and synthesize radiation-resistant ceramic materials applied in extremely radioactive environments.

ACKNOWLEDGMENTS

This work was supported by the National Natural Science Foundation of the People's Republic of China under Grant NOs. 11505122 and 11775152, the Science and Technology Innovation Team of Sichuan province under Grant NO.15CXTD0025, and the Key Applied Basic Research (2017JY0329) of Sichuan province. D.W. acknowledges the institutional funds from the Gene and Linda Voiland School of Chemical Engineering and Bioengineering at Washington State University. D. W. and X. G. also acknowledge the fund of the Alexandra Navrotsky Institute for Experimental Thermodynamics.

ORCID

Jianqi Qi https://orcid.org/0000-0002-6884-1258
Di Wu https://orcid.org/0000-0001-6879-321X

REFERENCES

1. Lang M, Zhang F, Zhang J, Wang J, Lian J, Weber WJ, et al. Review of $A_2B_2O_7$ pyrochlore response to irradiation and pressure. Nucl Instrum Meth B. 2010;268(19):2951–9.
2. Ewing RC. Nuclear waste disposal—pyrochlore ($A_2B_2O_7$): nuclear waste form for the immobilization of plutonium and "minor" actinides. J Appl Phys. 2004;95(11):5949.
3. Weber WJ, Ewing RC. Plutonium immobilization and radiation effects. Science. 2000;289(5487):2051–2.
4. Lian J, Chen J, Wang LM, Ewing RC, Farmer JM, Boatner LA, et al. Radiation-induced amorphization of rare-earth titanate pyrochlores. Phys Rev B. 2003;68(13):134107.
5. Lian J, Zu XT, Kutty KV, Chen J, Wang LM, Ewing RC. Ion-irradiation-induced amorphization of $La_2Zr_2O_7$ pyrochlore. Phys Rev B. 2002;66(5):054108.
6. Lang M, Zhang FX, Ewing RC, Lian J, Trautmann C, Wang Z. Structural modifications of $Gd_2Zr_{2-x}Ti_xO_7$ pyrochlore induced by swift heavy ions: disordering and amorphization. J Mater Res. 2011;24(04):1322–34.
7. Lu X, Ding Y, Shu X, Mao X, Wang X. Preparation and heavy-ion irradiation effects of $Gd_2Ce_xZr_{2-x}O_7$ceramics. RSC Adv. 2015;5(79):64247–53.
8. Taylor CA, Patel MK, Aguiar JA, Zhang Y, Crespillo ML, Wen J, et al. Bubble formation and lattice parameter changes resulting from He irradiation of defect-fluorite $Gd_2Zr_2O_7$. Acta Mater. 2016;115:115–22.
9. Kuri G, Döbeli M, Gavillet D. Damage evolution and surface morphology of helium implanted yttria-stabilized zirconia single crystal. Nucl Instrum Meth B. 2006;245(2):445–54.
10. Shen TD, Feng S, Tang M, Valdez JA, Wang Y, Sickafus KE. Enhanced radiation tolerance in nanocrystalline $MgGa_2O_4$. Appl Phys Lett. 2007;90(26):263115.
11. Dey S, Drazin JW, Wang Y, Valdez JA, Holesinger TG, Uberuaga BP, et al. Radiation tolerance of nanocrystalline ceramics: insights from Yttria Stabilized Zirconia. Sci Rep. 2015;5:7746.
12. Zhang J, Lian J, Fuentes AF, Zhang F, Lang M, Lu F, et al. Enhanced radiation resistance of nanocrystalline pyrochlore $Gd_2(Ti_{0.65}Zr_{0.35})_2O_7$. Appl Phys Lett. 2009;94(24):243110.
13. Hong M, Ren F, Zhang H, Xiao X, Yang B, Tian C, et al. Enhanced radiation tolerance in nitride multilayered nanofilms with small period-thicknesses. Appl Phys Lett. 2012;101(15):153117.

14. Barr CM, Li N, Boyce BL, Hattar K. Examining the influence of grain size on radiation tolerance in the nanocrystalline regime. Appl Phys Lett. 2018;112(18):181903.
15. Liu WB, Zhang JH, Ji YZ, Xia LD, Liu HP, Yun D, et al. Comparative study of He bubble formation in nanostructured reduced activation steel and its coarsen-grained counterpart. J Nucl Mater. 2018;500:213–9.
16. Sun C, Yu KY, Lee JH, Liu Y, Wang H, Shao L, et al. Enhanced radiation tolerance of ultrafine grained Fe–Cr–Ni alloy. J Nucl Mater. 2012;420(1–3):235–40.
17. Si S, Li W, Zhao X, Han M, Yue Y, Wu W, et al. Significant radiation tolerance and moderate reduction in thermal transport of a tungsten nanofilm by inserting monolayer grapheme. Adv Mater. 2017;29(3):1604623.
18. Huang ZY, Qi JQ, Zhou M, Gong Y, Shi Q, Yang M, et al. A facile solvothermal method for high-quality $Gd_2Zr_2O_7$ nanopowder preparation. Ceram Int. 2018;44(2):1334–42.
19. Devanathan R, Weber WJ. Simulation of collision cascades and thermal spikes in ceramics. Nucl Instrum Meth B. 2010;268(19):2857–62.
20. Qin W, Chen Z, Huang P, Zhuang Y. Crystal lattice expansion of nanocrystalline materials. J Alloy Compd. 1999;292(1–2):230–2.
21. Shen TD, Zhang JZ, Zhao YS. What is the theoretical density of a nanocrystalline material? Acta Mater. 2008;56(14):3663–71.
22. Sattonnay G, Sellami N, Thomé L, Legros C, Grygiel C, Monnet I, et al. Structural stability of $Nd_2Zr_2O_7$ pyrochlore ion-irradiated in a broad energy range. Acta Mater. 2013;61(17):6492–505.
23. Bai X, Voter A, Hoagland R, Nastasi M, Uberuaga B. Efficient annealing of radiation damage near grain boundaries via interstitial emission. Science. 2010;327(26):1631.
24. Dey S, Mardinly J, Wang Y, Valdez JA, Holesinger TG, Uberuaga BP, et al. Irradiation-induced grain growth and defect evolution in nanocrystalline zirconia with doped grain boundaries. Phys Chem Chem Phys. 2016;18(25):16921–9.
25. Uberuaga BP, Bacorisen D, Smith R, Ball JA, Grimes RW, Voter AF, et al. Defect kinetics in spinels: long-time simulations of $MgAl_2O_4$, $MgGa_2O_4$, and $MgIn_2O_4$. Phys Rev B. 2007;75(10):104116.
26. Yang T, Taylor CA, Wang C, Zhang Y, Weber WJ, Xiao J, et al. Effects of He irradiation on yttria-stabilized zirconia ceramics. J Am Ceram Soc. 2015;98(4):1314–22.
27. Shen TD. Radiation tolerance in a nanostructure: is smaller better? Nucl Instrum Meth B. 2008;266(6):921–5.
28. Meldrum A, Boatner LA, Ewing RC. Nanocrystalline zirconia can be amorphized by ion irradiation. Phys Rev Lett. 2002;88(2):025503.
29. Zhang Y, Jiang W, Wang C, Namavar F, Edmondson PD, Zhu Z, et al. Grain growth and phase stability of nanocrystalline cubic zirconia under ion irradiation. Phys Rev B. 2010;82(18):184105.
30. Wang C, Yang T, Kong S, Xiao J, Xue J, Wang Q, et al. Effects of He irradiation on Ti_3AlC_2: damage evolution and behavior of He bubbles. J Nucl Mater. 2013;440(1–3):606–11.

How to cite this article: Huang Z, Ma N, Qi J, et al. Defect-fluorite $Gd_2Zr_2O_7$ ceramics under helium irradiation: Amorphization, cell volume expansion, and multi-stage bubble formation. *J Am Ceram Soc*. 2019;102:4911–4918. https://doi.org/10.1111/jace.16364